


Fluctuation-Induced Interaction in Turbulent FlowsM. Davoodianidalik¹, H. Punzmann¹, H. Kellay², H. Xia¹, M. Shats¹, and N. Francois^{1,*}¹*Research School of Physics, The Australian National University, Canberra ACT 2601, Australia*²*Laboratoire Ondes et Matière d'Aquitaine, UMR 5798, CNRS, Université de Bordeaux, 33405 Talence, France* (Received 22 March 2021; revised 11 October 2021; accepted 15 December 2021; published 12 January 2022)

Fluctuation-induced forces are observed in numerous physical systems spanning from quantum to macroscopic scale. However, there is as yet no experimental report of their existence in hydrodynamic turbulence. Here, we present evidence of an attraction force mediated via turbulent fluctuations by using two walls locally confining 2D turbulence. This long-range interaction is a function of the wall separation and the energy injection rate in the turbulent flow. As the wall spacing decreases, the confined flow becomes less energetic and more anisotropic in the bounded domain, producing stronger attraction. The mechanism of force generation is rooted in a nontrivial fluid-wall coupling where coherent flow structures are guided by the cavity walls. For the narrowest cavities studied, a resonance phenomenon at the flow forcing scale leads to a complex short-range interaction. The results could be relevant to problems encountered in a range of fields from industrial multiphase flows to modeling of planetary formation.

DOI: [10.1103/PhysRevLett.128.024503](https://doi.org/10.1103/PhysRevLett.128.024503)

Turbulent flows exert a rich variety of forces on objects [1]: the lift force, the history force, or the added mass effect can make the dynamics of a single object in a turbulent flow very different from that of a fluid particle [2–6]. Among these forces of hydrodynamic origin, the description of interaction forces between nearby objects in turbulence is an outstanding question of physics. These forces remain poorly understood despite their relevance in many industrial and natural processes involving aggregation or fragmentation of objects in the presence of turbulence [7–9]. For instance, advances in our understanding of turbulence-induced interaction force might be beneficial to design efficient processes in industrial flows [4,9], to better control pulp fiber flocculation in the paper making industry [10], to model rock aggregation during planet formation [11], or to control flocs formation in biological fluids by using mesoscale turbulence [12–15].

While there have been remarkable advances in our understanding of collisional aggregation processes between microscopic particles carried by turbulence [4,7], relatively little is known about the ability of turbulent fluctuations to mediate attractive interaction forces between larger objects or particle aggregates. This lack is striking when compared to the continued research efforts devoted to fluctuation-induced forces and Casimir-like effects across various disciplines [16–22].

Hydrodynamic turbulence is a chaotic state of a macroscopic system generated and dominated by inertia. As such, the physical properties of turbulent fluctuations are quite singular and usually conceived as interacting eddies [1]. These eddies transfer energy via nonlinear interactions, in a process referred to as the energy cascade which occurs over a broad range of scales, the inertial range. Behind this

statistical description pioneered by Kolmogorov [23] hides a complex organization of turbulence in which coherent structures of different length scales coexist [24,25]. The interaction of this turbulent fabric with solid boundaries is a subject of intense research efforts and recent studies on the topic have uncovered interesting phenomena such as the control of turbulence by its destabilization in pipe flows [26], a fundamental link between the turbulent spectrum and wall friction drag [27,28], and the turbulence-driven propulsion [29–31]. Moreover, a recent numerical study has revealed the existence of a fluctuation-induced force between two solid plates immersed in homogeneous isotropic turbulence [32]. The emergence of this force was discussed in relation to a selective spatial filtering of diverse structures present in this ideal turbulent flow. However, in the framework of hydrodynamic turbulence, the physical mechanism responsible for fluctuation-induced forces and the physical parameters that control their magnitude remain poorly understood.

Here, we report an experimental observation of fluctuation-induced forces in laboratory hydrodynamic turbulence. The turbulent flow exerts a long-range attractive force on two walls forming a cavity that locally confines the hydrodynamic fluctuations. The reduction of kinetic energy and the anisotropy of the confined turbulence conspire to produce an attraction force. A key finding is that a single length scale controls both the growing asymmetry of the confined flow and the magnitude of the force. The attraction mechanism relies on the coupling of the cavity with the Lagrangian structure of the flow.

In these experiments, we use Faraday waves to produce turbulent fluid motion at a fluid surface in a 290-mm-diameter container [33–37]. The wave-driven turbulent

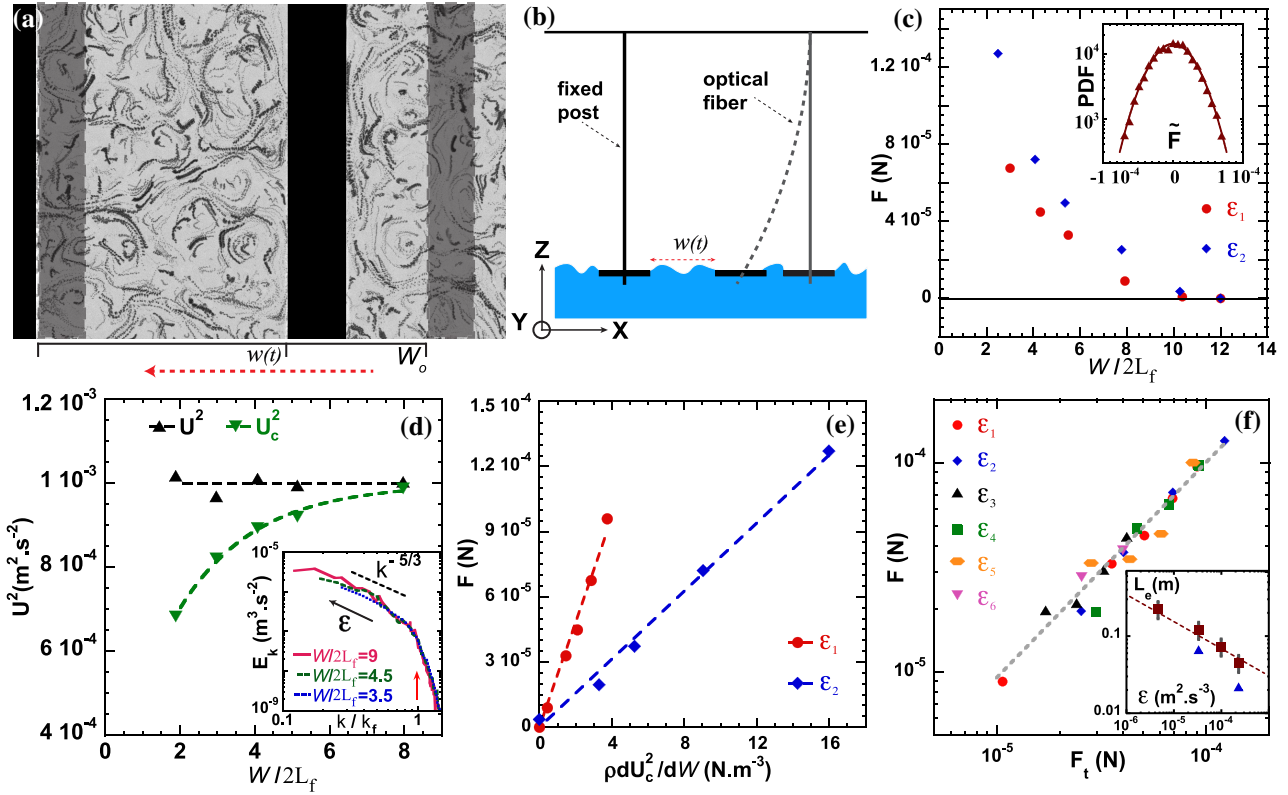


FIG. 1. Long-range turbulence-driven attraction force. (a) Two floating beams placed in wave-driven turbulence and initially separated by a distance W_0 attract each other (top view). Fluid particle streaks reveal the interacting eddies of the turbulent flow when the beams (black rectangles) instantaneous separation is $w(t) \approx 10L_f$. The gray rectangles indicate the initial and final relative positions of the beams. (b) Schematics of the experimental setup. (c) Attraction force F versus nondimensional mean separation $W/2L_f$. Both quantities are time averaged and shown for two energy injection rates ϵ ($\epsilon_1 < \epsilon_2$). Inset: PDF of the fluctuations \tilde{F} of the force. (d) Kinetic energies of the unbounded (U^2) and of the confined (U_c^2) turbulent flow versus $W/2L_f$ (at fixed $\epsilon = 2.5 \times 10^{-4} \text{ m}^2 \text{ s}^{-3}$). Inset: wave number spectra of the kinetic energy E_k of the confined flow for various degrees of confinement at fixed ϵ . (e) Experimentally measured force F versus $\rho \partial U_c^2 / \partial W$. (f) Force F as a function of the model $F_t = AL_e(\rho \partial U_c^2 / \partial W)$, where $A = L_b h$ and L_e is a free parameter ($L_b = 100 \text{ mm}$ for $\epsilon_{i=1,2,3,4}$, $L_b = 200 \text{ mm}$ for $\epsilon_{i=5,6}$). Inset: effective length scale L_e versus ϵ (red squares: $L_b = 100 \text{ mm}$; blue triangles: $L_b = 200 \text{ mm}$).

motion shows Gaussian velocity statistics, it has no mean flow component and its dynamics is slow compared to the wave frequency. This wave-driven turbulence shows striking similarities with 2D turbulence [38,39]. One essential aspect is the presence of an inverse energy cascade, or the transfer of energy from an intermediate forcing length scale L_f toward larger length scales. This process determines the kinetic energy $U^2 = U_x^2 + U_y^2$ of the horizontal flow. It is fueled by the generation and nonlinear interaction between horizontal vortices whose size is $L_f = \lambda/2$ where λ is the Faraday wave length [35,40,41] (in most experiments presented here $L_f = 4.4 \text{ mm}$). The energy injection rate ϵ into the horizontal turbulent flow is determined via spectral analysis of the flow kinetic energy. Floating beams are used to confine locally the turbulent flow. The beams are 3D printed and made of thermoplastic (acrylonitrile butadiene styrene). The density of the beams is adjusted to ensure that there is no meniscus on their edges

(see Supplemental Material [42]). A beam has a length in the range of $L_b = (50\text{--}200) \text{ mm}$, a width of 10 mm and a thickness of $h = 2 \text{ mm}$.

Figure 1(a) illustrates the central observation of our study: two floating rigid beams placed in the turbulent flow attract each other. To characterize this attraction force, we have used the experimental setup shown in Fig. 1(b). One beam is held in place by two rigid posts while the other is connected to two flexible optical fibers (see Supplemental Material [42]). In this configuration, the cavity formed by the beams confines the turbulent fluctuations and it is also dynamically coupled to the external turbulent flow via the moving beam. As they deform, the optical fiber cantilevers exert an elastic force on the moving beam. This force can be measured and it balances the hydrodynamic interaction force acting on the beam [30,43,44] (see Supplemental Material [42]). We investigated the evolution of this force as the beams are brought closer to each other. Figure 1(c) shows the interaction force F as a function of the beam

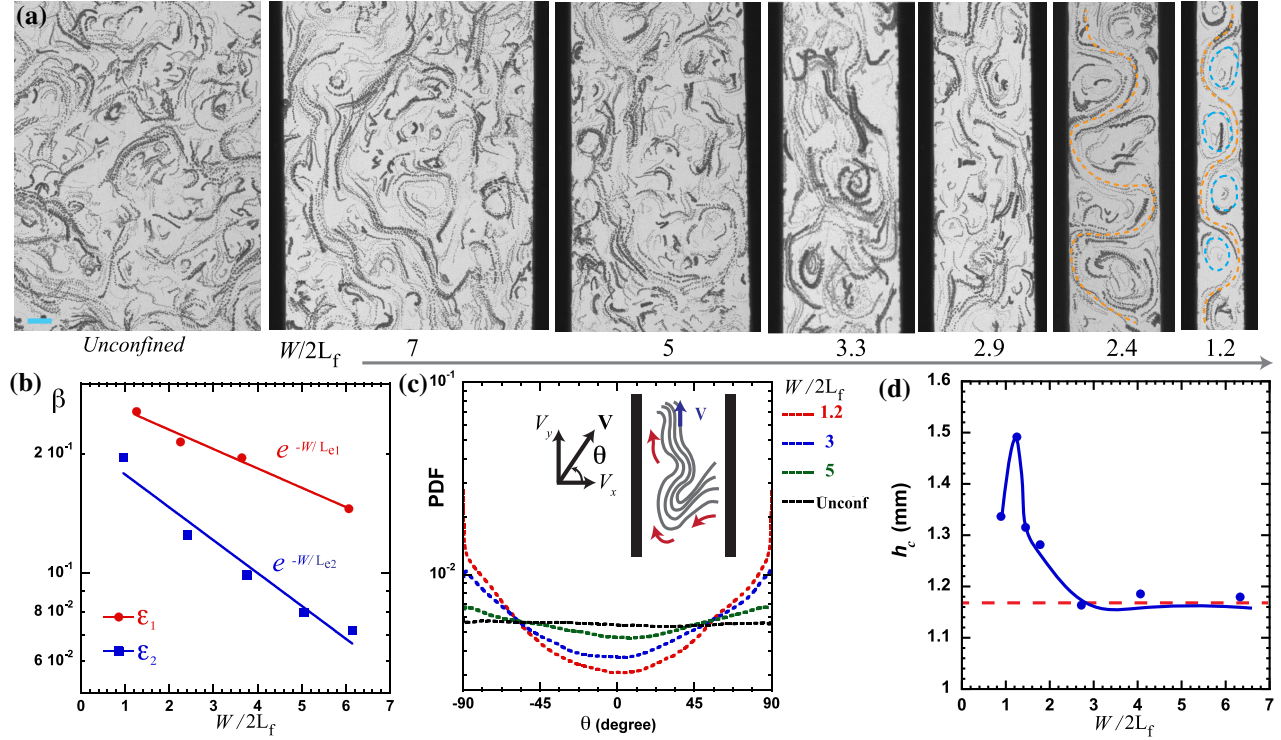


FIG. 2. Flow-cavity interaction. (a) Particle streaks show the evolution of the flow structure as the beam separation decreases. The light blue bar in the first panel indicates the typical width of the riverlike structures. At highest confinement, vortex cores and meandering rivers are highlighted using blue and orange dotted lines, respectively. (b) Flow asymmetry parameter $\beta = (U_y^2 - U_x^2)/U^2$ versus $W/2L_f$ for different energy injection rate $\epsilon_1 < \epsilon_2$. (c) PDF of the orientation θ of the fluid velocity \mathbf{V} for various gaps. Inset: illustration of the guiding of a riverlike structure within the cavity. (d) Root mean square wave amplitude h_c measured in the cavity versus gap width $W/2L_f$ at fixed $\epsilon = 3 \times 10^{-5} \text{ m}^2 \text{ s}^{-3}$. The red dotted line indicates the root mean square wave amplitude in unbounded wave-driven flows (see Supplemental Material [42]).

spacing W , both F and W are time-averaged quantities. The force is purely attractive (positive values) and shows a monotonic increase for decreasing values of the mean gap. An attraction force is detected for beam spacings much larger than the typical autocorrelation length $L_t \approx L_f \approx \lambda/2$ of the unbounded turbulent velocity field [45]. The fluctuations of the force follow a Gaussian distribution [see inset in Fig. 1(c)].

The horizontal fluid motion is turbulent on both sides of the moving beam [Fig. 1(a)]. In the domain bounded by the beams, the wave number spectrum of the flow kinetic energy shows a $k^{-5/3}$ scaling similar to that observed in the external ambient turbulence [see inset in Fig. 1(d)]. This signals the presence of the inverse energy cascade. While the geometrical confinement does not preclude the inverse energy cascade, it does reduce the magnitude of the turbulent kinetic energy U_c^2 in the bounded domain [see Fig. 1(d)]. This reduction of intensity of turbulent fluctuations invites analogies with Casimir-like effects.

In Fig. 1(e), we compare the force F to the derivative of the kinetic energy density with respect to the separation $\rho \partial U_c^2 / \partial W$ (which is the typical functional used to describe a Casimir effect [16]). The two quantities are found to be

linearly dependent, however, the slope of the relation depends on the energy injection rate ϵ in the turbulent flow. Figure 1(f) shows that the data can be collapsed onto a master curve when we use a model of the force in the form of $F_t = A L_e (\rho \partial U_c^2 / \partial W)$, where $A = L_b h$ is the area of the beams vertical cross section and L_e is a free parameter with the dimension of a length scale. L_e is a decreasing function of the energy injection rate ϵ , we find $L_e \sim \epsilon^{-1/3}$ [see inset in Fig. 1(f)].

We now discuss some features of the turbulence-driven attraction observed in these experiments. For large beam spacing $W > 3L_f$, a turbulent flow exists within the cavity [Fig. 2(a)]. The attraction force appears as a result of both the reduction of kinetic energy and the symmetry breaking of the confined turbulent flow. To quantify the latter effect, we use the parameter $\beta = (U_y^2 - U_x^2)/U^2$ [see Figs. 2(b) and 2(c)], which is zero in unbounded turbulence. When computed in the cavity, β increases exponentially with the decrease in the separation as $\beta \approx \exp(-W/L_e)$. The length L_e used in the force model, thus incorporates the symmetry breaking of the flow due to confinement in the direction transverse to the wall. Moreover, the anisotropy of the confined turbulence decreases with the increase of ϵ

[Fig. 2(b)]. The length scale L_e is substantially larger than the spatial autocorrelation length scale L_t of the velocity field in unbounded turbulence [45], taking values as high as $L_e \approx 20L_t$. This highlights the long-range nature of the interaction mediated by the turbulent fluctuations.

The physical mechanism driving the growing flow asymmetry is related to the coupling of the Lagrangian structure of the flow with the cavity walls. The wave-driven turbulence is composed of Lagrangian coherent structures, made of nondiverging bundles of fluid particles, resembling rivers [29,46]. In unbounded turbulence, such rivers have a mean contour (Lagrangian) length of about $30L_f$. Figure 2(a) captures how these rivers are progressively guided by the beam as the separation becomes smaller. The guiding effect appears for beam spacings W much larger than the typical width of the coherent structures which is roughly equal to $L_t \approx L_f$ [29,46]. This long-range effect is also evident in the changes of the probability density function (PDF) of the fluid velocity orientation as the cavity becomes narrower [Fig. 2(c)]. Recently, it has been shown that such a wall-guiding effect can produce turbulent-driven propulsion when walls are curved and the geometrical confinement is only partial [29,30]. In the case of straight walls, the collisions of rivers with the two sides of the beam produces a momentum transfer. In our modeling, the force reads as $F_t \sim L_e \times \partial U_c^2 / \partial W$. The second factor describes the imbalance between the momentum carried by the external rivers versus that of the confined rivers. The length L_e conveys that the more aligned the rivers are with the walls, the less efficient is the momentum transfer by the confined rivers giving rise to a stronger attraction.

The length scale L_e reflects a competition between the flow anisotropy induced by the walls and the randomization of the rivers' orientation due to the turbulent agitation. The latter can be modeled as a random process whose diffusion coefficient is proportional to the flow velocity $U \sim \epsilon^{1/3}$ [45,46]. Consequently, the level of flow anisotropy in the cavity decreases with an increase in ϵ and we observe the scaling $L_e \sim \epsilon^{-1/3}$. The mechanism producing the attraction force shows similarities with different self-propulsion phenomena observed in wave-driven turbulence [29–31]. These studies describe propulsive forces F_p and a relation $F_p \sim U^2/U$, where the U^2 term is related to the guiding of the rivers by a curved wall while the factor $1/U$ reflects an adverse effect to propulsion due to the turbulent randomization of the river motion.

Since the 2D turbulent flows are driven by Faraday waves, it is natural to ask whether the attraction force could be alternatively described as an effect mediated by the fluctuations of the wave amplitude. As shown in Fig. 2(d), when $W/2L_f > 2.5$, the root mean square wave amplitudes measured within and outside the cavity are identical. According to the model of wave-mediated force developed in [47], there should be no interaction between the beams at

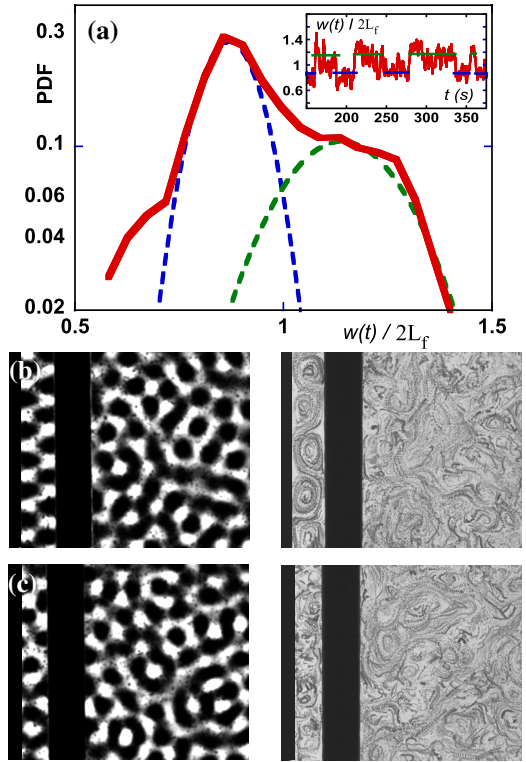


FIG. 3. High-confinement regime. (a) PDF of the instantaneous gap $w(t)$ when the mean separation is $W \sim 2L_f$. The PDF can be modeled by two Gaussian distributions centered on w_1 and w_2 with different variances. Inset: dynamics of the time-varying gap $w(t)$. (b),(c) Diffusing light image (left panels) of the resonant wave mode (b) and disordered waves (c). The right panels show associated flows.

large separation. Only a short-range ($W/2L_f < 0.5$) wave-mediated attraction was reported in [47]; indeed no wave-driven hydrodynamic turbulence could be generated in these experiments due to the strong confinement of the wave field imposed by the small container size (see Supplemental Material [42]). In our experiments, 2D turbulence governs both the fluid particle motion and the disorder in the wave field [35,48].

When the beam spacing is larger than $3L_f$, the balance of the fluctuation-induced attraction and the elastic restoring force produces a cavity with a stable width W . As the separation decreases to values close to the forcing scale ($0.7L_f < W < 3L_f$), wave-driven ordered and disordered flows conspire to produce a complex short-range interaction between the beams [Fig. 2(a)]. The inset of Fig. 3(a) illustrates the typical dynamics of the instantaneous separation distance $w(t)$ in this regime. It shows that the moving wall remains stable around $w_1 \approx 2.4L_f$ or $w_2 \approx 1.6L_f$ for extended periods of time. This dynamics results in a bimodal PDF of the distance $w(t)$. This bistability is related to the emergence of strong wave resonance events with finite lifetime [Figs. 2(d), 3(b), and 3(c); see Supplemental Material [42]]. More precisely, we observe

successive transitions in the wave spatial structure between a disordered and an ordered state. The latter consists of a periodic wave pattern which is reminiscent of a resonant mode of an optical cavity [see Fig. 3(b)]. The disordered state is characterized by unstable waves of which a transient motif is shown in Fig. 3(c). Each wave state has a clear signature on the structure of the confined flow. The resonant mode generates a periodic alley of vortices while the disordered state produces a chaotic flow. There is a direct connection between the two flow states and the metastable positions of the moving beam. The periodic flow has a high kinetic energy and generates the largest separation w_1 , it is associated with a weaker attraction than the less energetic chaotic flow observed when the beam separation is w_2 (see Supplemental Material [42]). The Lagrangian structure of the periodic flow is composed of two elements: vortex cores coexisting with riverlike structures [Fig. 2(a)]. The transient rivers are meandering in between the vortex cores; they are guided by both the beams and the vortex cores. We note that the vortex cores have a typical diameter of L_f . From the flow viewpoint, the alley of vortices could therefore be considered as a resonance of the forcing mechanism of the flow [35]. The typical lifetime of a resonant event is about $200T_L$, where $T_L \approx 0.1$ s is the autocorrelation time of velocity fluctuations in unbounded turbulence [45]. Observing such a persistent resonance phenomenon in our system is remarkable since the confining cavity is coupled to the external turbulence via the motion of one of its walls. In this regime, the system seems to act as a self-tuning resonator reinforcing the lifetime of the resonant events.

Summarizing, these experiments shed light on an interaction force mediated by hydrodynamic turbulent fluctuations. Our study shows how the reduction of kinetic energy and the symmetry breaking of the confined turbulence produce an attraction force. The long-range attraction mechanism based on the confinement of Lagrangian coherent structures may lead to a better understanding of aggregation phenomena observed in engineering processes [3,7,10] or in plankton blooming at the surface of the oceans [49].

This work was supported by the Australian Research Council Discovery Projects and Linkage Projects funding scheme (DP160100863, DP190100406, and LP160100477). N.F. acknowledges support by the Australian Research Council's DECRA Grant (No. 160100742). H. X. acknowledges support from the Australian Research Council Future Fellowship (No. FT140100067).

* nicolas.francois@anu.edu.au

[1] H. Tennekes and J. L. Lumley, *A First Course in Turbulence* (MIT Press, Cambridge, Massachusetts, 1972).

- [2] M. R. Maxey and J. J. Riley, Equation of motion for a small rigid sphere in a nonuniform flow, *Phys. Fluids* **26**, 883 (1983).
- [3] V. Mathai, D. Lohse, and C. Sun, Bubbly and buoyant particle-laden turbulent flows, *Annu. Rev. Condens. Matter Phys.* **11**, 529 (2020).
- [4] F. Toschi and E. Bodenschatz, Lagrangian properties of particles in Turbulence, *Annu. Rev. Fluid Mech.* **41**, 375 (2009).
- [5] R. P. Ojha, P.-A. Lemieux, P. K. Dixon, A. J. Liu, and D. J. Durian, Statistical mechanics of a gas-fluidized particle, *Nature (London)* **427**, 521 (2004).
- [6] C. Brouzet, G. Verhille, and P. Le Gal, Flexible Fiber in a Turbulent Flow: A Macroscopic Polymer, *Phys. Rev. Lett.* **112**, 074501 (2014).
- [7] A. Pumir and M. Wilkinson, Collisional aggregation due to turbulence, *Annu. Rev. Condens. Matter Phys.* **7**, 141 (2016).
- [8] H. M. De La Rosa Zambrano, G. Verhille, and P. Le Gal, Fragmentation of magnetic particle aggregates in turbulence, *Phys. Rev. Fluids* **3**, 084605 (2018).
- [9] B. Oyegebile, P. Ay, and S. Narra, Flocculation kinetics and hydrodynamic interactions in natural and engineered flow systems: A review, *Env. Eng. Res.* **21**, 1 (2016).
- [10] F. Lundell, L. D. Soderberg, and P. H. Alfredsson, Fluid mechanics of papermaking, *Annu. Rev. Fluid Mech.* **43**, 195 (2011).
- [11] J. Blum and G. Wurm, The growth mechanisms of macroscopic bodies in protoplanetary disks, *Annu. Rev. Astron. Astrophys.* **46**, 21 (2008).
- [12] G. Kokot, S. Das, R. G. Winkler, G. Gompper, I. S. Aranson, and A. Snezhko, Active turbulence in a gas of self-assembled spinners, *Proc. Natl. Acad. Sci. U.S.A.* **114**, 12870 (2017).
- [13] K. Han, G. Kokot, S. Das, R. G. Winkler, G. Gompper, and A. Snezhko, Reconfigurable structure and tunable transport in synchronized active spinner materials, *Sci. Adv.* **6**, 12 (2020).
- [14] S.-H. Hong, J. Yang, M. Davoodianidalik, H. Punzmann, M. Shats, and H. Xia, Turbulence-assisted formation of bacterial cellulose, [arXiv:2009.06208](https://arxiv.org/abs/2009.06208).
- [15] M. Linkmann, G. Boffetta, M. C. Marchetti, and B. Eckhardt, Phase Transition to Large Scale Coherent Structures in Two-Dimensional Active Matter Turbulence, *Phys. Rev. Lett.* **122**, 214503 (2019).
- [16] M. Kardar and R. Golestanian, The friction of vacuum, and other fluctuation-induced forces, *Rev. Mod. Phys.* **71**, 1233 (1999).
- [17] H. B. Casimir, On the attraction between two perfectly conducting plates, *Proc. K. Ned. Akad. Wet.* **51**, 793 (1948).
- [18] D. Bonn, J. Otwinowski, S. Sacanna, H. Guo, G. Weddam, and P. Schall, Direct Observation of Colloidal Aggregation by Critical Casimir Forces, *Phys. Rev. Lett.* **103**, 156101 (2009).
- [19] D. Ray, C. Reichhardt, and C. J. Olson Reichhardt, Casimir effect in active matter systems, *Phys. Rev. E* **90**, 013019 (2014).
- [20] C. Hertlein, L. Helden, A. Gambassi, S. Dietrich, and C. Bechinger, Direct measurement of critical Casimir forces, *Nature (London)* **451**, 172 (2008).

- [21] A. A. Lee, D. Vella, and J. S. Wettlaufer, Fluctuation spectra and force generation in nonequilibrium systems, *Proc. Natl. Acad. Sci. U.S.A.* **114**, 9255 (2017).
- [22] I. Zuriguel, J. F. Boudet, Y. Amarouchene, and H. Kellay, Role of Fluctuation-Induced Interactions in the Axial Segregation of Granular Materials, *Phys. Rev. Lett.* **95**, 258002 (2005).
- [23] A. N. Kolmogorov, The local structure of turbulence in incompressible viscous fluid for very large Reynolds numbers, *Dokl. Akad. Nauk SSSR* **30**, 301 (1941).
- [24] S. Douady, Y. Couder, and M. E. Brachet, Direct Observation of the Intermittency of Intense Vorticity Filaments in Turbulence, *Phys. Rev. Lett.* **67**, 983 (1991).
- [25] A. Pumir, A numerical study of pressure fluctuations in three-dimensional, incompressible, homogeneous, isotropic turbulence, *Phys. Fluids* **6**, 2071 (1994).
- [26] J. Kuhnen, B. Song, D. Scarselli, N. B. Budanur, M. Riedl, A. P. Willis, M. Avila, and B. Hof, Destabilizing turbulence in pipe flow, *Nat. Phys.* **14**, 386 (2018).
- [27] T. Tran, P. Chakraborty, N. Guttenberg, A. Prescott, H. Kellay, W. Goldberg, N. Goldenfeld, and G. Gioia, Macroscopic effects of the spectral structure in turbulent flows, *Nat. Phys.* **6**, 438 (2010).
- [28] A. Vilquin, J. Jagielka, S. Djambov, H. Herouard, P. Fischer, C-H. Bruneau, P. Chakraborty, G. Gioia, and H. Kellay, Asymptotic turbulent friction in 2D rough-walled flows, *Sci. Adv.* **7**, 5 (2021).
- [29] N. Francois, H. Xia, H. Punzmann, and M. Shats, Rectification of chaotic fluid motion in two-dimensional turbulence, *Phys. Rev. Fluids* **3**, 124602 (2018).
- [30] J. Yang, M. Davoodianidalik, H. Xia, H. Punzmann, M. Shats, and N. Francois, Passive propulsion in turbulent flows, *Phys. Rev. Fluids* **4**, 104608 (2019).
- [31] N. Francois, H. Xia, H. Punzmann, and M. Shats, Non-equilibrium Thermodynamics of Turbulence-Driven Rotors, *Phys. Rev. Lett.* **124**, 254501 (2020).
- [32] V. Spandan, D. Putt, R. Ostilla-Monico, and A. A. Lee, Fluctuation-induced force in homogeneous isotropic turbulence, *Sci. Adv.* **6**, 14 (2020).
- [33] N. Francois, H. Xia, H. Punzmann, and M. Shats, Inverse Energy Cascade and Emergence of Large Coherent Vortices in Turbulence Driven by Faraday Waves, *Phys. Rev. Lett.* **110**, 194501 (2013).
- [34] A. von Kameke, F. Huhn, G. Fernandez-Garcia, A. P. Munuzuri, and V. Perez-Munuzuri, Double Cascade Turbulence and Richardson Dispersion in a Horizontal Fluid Flow Induced by Faraday Waves, *Phys. Rev. Lett.* **107**, 074502 (2011).
- [35] N. Francois, H. Xia, H. Punzmann, S. Ramsden, and M. Shats, Three-Dimensional Fluid Motion in Faraday Waves: Creation of Vorticity and Generation of Two-Dimensional Turbulence, *Phys. Rev. X* **4**, 021021 (2014).
- [36] R. Colombi, M. Schluter, and A. von Kameke, Three dimensional flows beneath a thin layer of 2D turbulence induced by Faraday waves, *Exp. Fluids* **62**, 8 (2021).
- [37] H. Xia and N. Francois, Two-dimensional turbulence in three-dimensional flows, *Phys. Fluids* **29**, 111107 (2017).
- [38] R. Kraichnan, Inertial ranges in two-dimensional turbulence, *Phys. Fluids* **10**, 1417 (1967).
- [39] G. Boffetta and R. E. Ecke, Two-dimensional turbulence, *Annu. Rev. Fluid Mech.* **44**, 427 (2012).
- [40] S. V. Filatov, V. M. Parfenyev, S. S. Vergeles, M. Yu. Brazhnikov, A. A. Levchenko, and V. V. Lebedev, Nonlinear Generation of Vorticity by Surface Waves, *Phys. Rev. Lett.* **116**, 054501 (2016).
- [41] N. Francois, H. Xia, H. Punzmann, F. W. Fontana, and M. Shats, Wave-based liquid-interface metamaterials, *Nat. Commun.* **8**, 14325 (2017).
- [42] See Supplemental Material at <http://link.aps.org/supplemental/10.1103/PhysRevLett.128.024503> for details on experimental methods, flow characterization, production of the floating beams, measurement protocol of the attraction force using optical fiber cantilevers and additional information on the wave and fluid particle dynamics in wave-driven turbulence.
- [43] H. Kellay, X-L Wu, and W. I. Goldberg, Experiments with Turbulent Soap Films, *Phys. Rev. Lett.* **74**, 3975 (1995).
- [44] N. Francois, D. Lasne, Y. Amarouchene, B. Lounis, and H. Kellay, Drag Enhancement with Polymers, *Phys. Rev. Lett.* **100**, 018302 (2008).
- [45] H. Xia, N. Francois, H. Punzmann, and M. Shats, Lagrangian scale of particle dispersion in turbulence, *Nat. Commun.* **4**, 2013 (2013).
- [46] H. Xia, N. Francois, H. Punzmann, and M. Shats, Tunable diffusion in wave-driven two-dimensional turbulence, *J. Fluid Mech.* **865**, 811 (2019).
- [47] B. C. Denardo, J. J. Puda, and A. Larraza, A water wave analog of the Casimir effect, *Am. J. Phys.* **77**, 1095 (2009).
- [48] N. Francois, H. Xia, H. Punzmann, and M. Shats, Wave-particle interaction in the Faraday waves, *Eur. Phys. J. E* **38**, 106 (2015).
- [49] T. Kiorboe, *A Mechanistic Approach to Plankton Ecology* (Princeton University Press, Princeton, NJ, 2008).